

# Vortex Core Structure and Dynamics in Layered Superconductors

M. Eschrig<sup>1,2</sup>, D. Rainer<sup>3</sup>, and J. A. Sauls<sup>1</sup>

<sup>1</sup> Department of Physics, Northwestern University, Evanston, IL 60208, USA

<sup>2</sup> Materials Science Division, Argonne National Laboratory, Argonne, IL 60439, USA

<sup>3</sup> Physikalisches Institut, Universität Bayreuth, D-95440 Bayreuth, Germany

**Abstract.** We investigate the equilibrium and nonequilibrium properties of the core region of vortices in layered superconductors. We discuss the electronic structure of singly and doubly quantized vortices for both *s*-wave and *d*-wave pairing symmetry. We consider the intermediate clean regime, where the vortex-core bound states are broadened into resonances with a width comparable to or larger than the quantized energy level spacing, and calculate the response of a vortex core to an *a.c.* electromagnetic field for vortices that are pinned to a metallic defect. We concentrate on the case where the vortex motion is nonstationary and can be treated by linear response theory. The response of the order parameter, impurity self energy, induced fields and currents are obtained by a self-consistent calculation of the distribution functions and the excitation spectrum. We then obtain the dynamical conductivity, spatially resolved in the region of the core, for external frequencies in the range,  $0.1\Delta < \hbar\omega \lesssim 3\Delta$ . We also calculate the dynamically induced charge distribution in the vicinity of the core. This charge density is related to the nonequilibrium response of the bound states and collective mode, and dominates the electromagnetic response of the vortex core.

## 1 Introduction

Vortex motion is the principle mechanism for resistive losses in type II superconductors. Vortices also provide valuable information about the nature of low lying excitations in the superconducting state. In clean *s*-wave BCS superconductors the low-lying excitations in the core are the bound states of Caroli, de Gennes and Matricon [1]. These excitations have superconducting as well as normal metallic properties. For example, these states are the source of circulating supercurrents in the equilibrium vortex core, and they are strongly coupled to the condensate by Andreev scattering [2,3]. Furthermore, the response of the vortex core states to an electromagnetic field is generally very different from that of normal electrons. However, in the dirty limit,  $\hbar/\tau \gg \Delta$ , the Bardeen-Stephen model [4] of a normal-metal spectrum with the local Drude conductivity in the core provides a reasonable description of the dissipative dynamics of the vortex core. The opposite extreme is the “superclean limit”,  $\hbar/\tau \ll \Delta^2/E_f$ , in which the quantization of the vortex-core bound states must be taken into account. In this limit a single impurity and its interaction with the vortex core states must be considered. The *a.c.* electromagnetic response is then controlled by selection rules governing transition matrix elements for the quantized core levels and the

level structure of the core states in the presence of an impurity [5,6,7]. In the case of d-wave superconductors in the superclean limit, *nodes* in the spectrum of bound states lead to a finite dissipation from Landau damping for  $T \rightarrow 0$  [8].

The superclean limit is difficult to achieve even for short coherence length superconductors; weak disorder broadens the vortex core levels into a quasi-continuum. We investigate the intermediate-clean regime,  $\Delta^2/E_f \ll \hbar/\tau \ll \Delta$ , where the discrete level structure of the vortex-core states is broadened and the selection rules are broken due to strong overlap between the bound state wave functions. However, the vortex core states remain well defined on the scale of the superconducting gap,  $\Delta$ . In this regime we can take advantage of the power of the quasiclassical theory of nonequilibrium superconductivity [9,10,11,12,13].

The energy required to maintain a net charge density of order an elementary charge per particle within a coherence volume (or coherence area in two dimensions) is much larger than the condensation energy. Thus, charge accumulation in the vortex core is strongly suppressed. In order to reduce the Coulomb energy associated with the charge accumulation an internal electrochemical potential,  $\Phi(\mathbf{R}; t)$ , develops in response to an external electric field. This potential produces an internal electric field,  $\mathbf{E}^{\text{int}}(\mathbf{R}; t)$ , which is the same order of magnitude as the external field. Even though the external field may vary on a scale that is large compared to the coherence length,  $\xi_0$ , the internal field develops on the coherence length scale. The source of the internal field is a charge density that accumulates inhomogeneously over length scales of order the coherence length. It is necessary to calculate the induced potential self consistently from the spatially varying order parameter, spectral function and distribution function for the electronic states in the vicinity of the vortex core. An order of magnitude estimate shows that to produce an induced field of the order of the external field, the dynamically induced charge is of order  $e (\Delta/E_f)(\delta v_\omega/\Delta)$ , where  $\delta v_\omega \sim eE^{\text{ext}}/\xi_0\omega$  is the typical energy scale set by the strength of the external field. This charge density accumulates predominantly in the vortex core region and creates a dipolar field around the vortex core. For a pinned vortex the charge accumulates near the interface separating the metallic inclusion from the superconductor.

Disorder plays a central role in the dissipative dynamics of the mixed state of type II superconductors. Impurities and defects are a source of scattering that limits the mean free path of carriers, thus increasing the resistivity. Defects also provide ‘pinning sites’ that inhibit vortex motion and suppresses the flux-flow resistivity. However, for *a.c.* fields even pinned vortices are sources for dissipation. The magnitude and frequency dependence of this dissipation depends on the electronic structure and dynamics of the core states of the pinned vortex. In the analysis presented below we consider vortices in the presence of pinning centers. We model a pinning center as a normal metallic inclusion which is coupled to the electronic states of the superconductor through a highly transmitting interface. In this model the charge dynamics of the electronic states near the interface between the pinning region and superconductor plays an important role in the electromagnetic response of the core.

In the next section we provide a short summary of the nonequilibrium quasiclassical equations, including the transport equations for the quasiparticle distribution and spectral functions, constitutive equations for the order parameter, impurity self-energy and electromagnetic potentials. In section 3 we present calculations for the electronic structure of vortices for superconductors with both *s*-wave and *d*-wave pairing symmetry. The results are based on self-consistent calculations of the order parameter and impurity self energy. For *s*-wave superconductors, impurity scattering leads to inhomogeneous broadening of the vortex core bound states, as well as bands of impurity states within the gap. In the case of *d*-wave pairing the core states are further broadened by coupling between bound states and the continuum states through impurity scattering. We also discuss the structure of doubly quantized vortices and vortices bound to mesoscopic size metallic inclusions. In the case of the doubly quantized vortex there are two branches of zero-energy bound states centered at finite impact parameter from the vortex center. This leads to a unique signature of a doubly quantized vortex: currents in the core circulate opposite to the supercurrents outside the core. Section 4 summarizes calculations of the vortex core dynamics for *s*-wave vortices in the presence of impurity scattering. We describe the charge dynamics of the vortex core for both pinned and unpinned vortices, and calculate the local a.c. conductivity that results from the coupled dynamics of the order parameter collective mode and the quasiparticle bound states in the vortex core. We discuss energy transport by the core states and the absorption features in the conductivity spectrum, which we interpret in terms of absorption within the bound-state band centered at the Fermi level and resonant transitions involving the bound and continuum states.

## 2 Nonequilibrium Transport Equations

The quasiclassical theory describes equilibrium and nonequilibrium properties of superconductors on length scales that are large compared to microscopic scales (i.e. the lattice constant, Fermi wavelength,  $k_f^{-1}$ , Thomas-Fermi screening length, etc.) and energies that are small compared to the atomic scales (e.g. Fermi energy,  $E_f$ , plasma frequency, conduction band width, etc.). Thus, there are small dimensionless parameters that define the limits of validity of the quasiclassical theory. In particular, we require  $k_f \xi_0 \gg 1$ ,  $k_B T_c / E_f \ll 1$  and  $\hbar \omega \ll E_f$ , where the a.c. frequencies of interest are typically of order  $\Delta \sim T_c$ , or smaller, and the length scales of interest are of order the coherence length,  $\xi_0 = \hbar v_f / 2\pi k_B T_c$ , or longer. Hereafter we use units in which  $\hbar = k_B = 1$ , and adopt the sign convention  $e = -|e|$  for the electron charge.

In quasiclassical theory quasiparticle wavepackets move along nearly straight, classical trajectories at the Fermi velocity. The classical dynamics of the quasiparticle excitations is governed by semi-classical transport equations for their phase-space distribution function. The quantum mechanical degrees of freedom are the “spin” and “particle-hole degree of freedom”, described by  $4 \times 4$  density matrices (Nambu matrices). The quantum dynamics is coupled to the classical

dynamics of the quasiparticles in phase space through the matrix structure of the quasiclassical transport equations.

The nonequilibrium quasiclassical transport equations [9,10,11,12,13] are formulated in terms of a quasiclassical Nambu-Keldysh propagator  $\check{g}(\mathbf{p}_f, \mathbf{R}; \epsilon, t)$ , which is a matrix in the combined Nambu-Keldysh space, and is a function of position  $\mathbf{R}$ , time  $t$ , energy  $\epsilon$ , and momenta  $\mathbf{p}_f$  on the Fermi surface.<sup>1</sup> We denote Nambu-Keldysh matrices by a “check”, and their  $4 \times 4$  Nambu submatrices of *advanced* (A), *retarded* (R) and Keldysh-type (K) propagators by a “hat”. The Nambu-Keldysh matrices for the quasiclassical propagator and self-energy have the form,

$$\check{g} = \begin{pmatrix} \hat{g}^R & \hat{g}^K \\ 0 & \hat{g}^A \end{pmatrix}, \quad \check{\sigma} = \begin{pmatrix} \hat{\sigma}^R & \hat{\sigma}^K \\ 0 & \hat{\sigma}^A \end{pmatrix}, \quad (1)$$

where  $\hat{g}^{R,A,K}$  are the retarded (R), advanced (A) and Keldysh (K) quasiclassical propagators, and similarly for the self-energy functions. Each of these components of  $\check{g}$  and  $\check{\sigma}$  are  $4 \times 4$  Nambu matrices in combined particle-hole-spin space. For a review of the methods and an introduction to the notation we refer to Refs. [15,14,16]. In the compact Nambu-Keldysh notation the transport equations and the normalization conditions read

$$\left[ \left( \epsilon + \frac{e}{c} \mathbf{v}_f \cdot \mathbf{A} \right) \check{\tau}_3 - e Z_0 \Phi \check{1} - \check{\Delta}_{mf} - \check{\nu}_{mf} - \check{\sigma}_i, \check{g} \right]_{\otimes} + i \mathbf{v}_f \cdot \nabla \check{g} = 0, \quad (2)$$

$$\check{g} \otimes \check{g} = -\pi^2 \check{1}, \quad (3)$$

where the commutator is  $[\check{A}, \check{B}]_{\otimes} = \check{A} \otimes \check{B} - \check{B} \otimes \check{A}$ ,

$$\check{A} \otimes \check{B}(\epsilon, t) = e^{\frac{i}{2}(\partial_{\epsilon}^A \partial_t^B - \partial_t^A \partial_{\epsilon}^B)} \check{A}(\epsilon, t) \check{B}(\epsilon, t). \quad (4)$$

The vector potential,  $\mathbf{A}(\mathbf{R}; t)$ , includes  $\mathbf{A}_0(\mathbf{R})$  which generates the static magnetic field,  $\mathbf{B}_0(\mathbf{R}) = \nabla \times \mathbf{A}_0(\mathbf{R})$ , as well as the non-stationary vector potential describing the time-varying electromagnetic field;  $\check{\Delta}_{mf}(\mathbf{p}_f, \mathbf{R}; t)$  is the mean-field order parameter matrix,  $\check{\nu}_{mf}(\mathbf{p}_f, \mathbf{R}; t)$  describes diagonal mean fields due to quasiparticle interactions (Landau interactions), and  $\check{\sigma}_i(\mathbf{p}_f, \mathbf{R}; \epsilon, t)$  is the impurity self-energy. The electrochemical potential  $\Phi(\mathbf{R}; t)$  includes the field generated by the induced charge density,  $\rho(\mathbf{R}; t)$ . The coupling of quasiparticles to the external potential involves virtual high-energy processes, which result from polarization of the non-quasiparticle background. The interaction of quasiparticles with both the external potential  $\Phi$  and the polarized background can be described by coupling to an effective potential  $Z_0 \Phi$  [14]. The high-energy renormalization factor  $Z_0$  is defined below in Eq. (12). The coupling of the quasiparticle current to the vector potential in Eq. (2) is given in terms of the quasiparticle Fermi velocity. No additional renormalization is needed to account for the effective coupling of the charge current to the vector potential because the renormalization by the non-quasiparticle background is accounted for by

<sup>1</sup> In quasiclassical theory the description in terms of the variables  $(\epsilon, \mathbf{p}_f, \mathbf{R})$  is related to the phase-space description in  $\mathbf{p} - \mathbf{R}$  space by a transformation,  $g(\mathbf{p}_f, \epsilon; \mathbf{R}, t) = f(\mathbf{p}, \mathbf{R}; t)$ , with  $\epsilon = \varepsilon(\mathbf{p}, \mathbf{R}; t) - \mu$  and  $\hat{\mathbf{p}} = \hat{\mathbf{p}}_f$  [14].

the effective potentials that determine the band structure, and therefore the quasiparticle Fermi velocity.

## 2.1 Constitutive Equations

Equations (2-3) must be supplemented by Maxwell's equations for the electromagnetic potentials, and by self-consistency equations for the order parameter and the impurity self-energy. We use the weak-coupling gap equation to describe the superconducting state, including unconventional pairing. The mean field self energies are then given by,

$$\hat{\Delta}_{mf}^{R,A}(\mathbf{p}_f, \mathbf{R}; t) = N_f \int_{-\epsilon_c}^{+\epsilon_c} \frac{d\epsilon}{4\pi i} \langle V(\mathbf{p}_f, \mathbf{p}'_f) \hat{f}^K(\mathbf{p}'_f, \mathbf{R}; \epsilon, t) \rangle, \quad (5)$$

$$\hat{\nu}_{mf}^{R,A}(\mathbf{p}_f, \mathbf{R}; t) = N_f \int_{-\epsilon_c}^{+\epsilon_c} \frac{d\epsilon}{4\pi i} \langle A(\mathbf{p}_f, \mathbf{p}'_f) \hat{g}^K(\mathbf{p}'_f, \mathbf{R}; \epsilon, t) \rangle, \quad (6)$$

$$\hat{\Delta}_{mf}^K(\mathbf{p}_f, \mathbf{R}; t) = 0, \quad \hat{\nu}_{mf}^K(\mathbf{p}_f, \mathbf{R}; t) = 0. \quad (7)$$

The impurity self-energy,

$$\check{\sigma}_i(\mathbf{p}_f, \mathbf{R}; \epsilon, t) = n_i \check{t}(\mathbf{p}_f, \mathbf{p}_f, \mathbf{R}; \epsilon, t), \quad (8)$$

is specified by the impurity concentration,  $n_i$ , and impurity scattering  $t$ -matrix, which is obtained from the self-consistent solution of the  $t$ -matrix equations,

$$\begin{aligned} \check{t}(\mathbf{p}_f, \mathbf{p}'_f, \mathbf{R}; \epsilon, t) &= \check{u}(\mathbf{p}_f, \mathbf{p}'_f) \\ &+ N_f \langle \check{u}(\mathbf{p}_f, \mathbf{p}'_f) \otimes \check{g}(\mathbf{p}'_f, \mathbf{R}; \epsilon, t) \otimes \check{t}(\mathbf{p}'_f, \mathbf{p}'_f, \mathbf{R}; \epsilon, t) \rangle. \end{aligned} \quad (9)$$

The Nambu matrix  $\hat{f}^K$  is the off-diagonal part of  $\hat{g}^K$ , while  $\hat{g}^K$  is the diagonal part in particle-hole space. The Fermi surface average is defined by

$$\langle \dots \rangle = \frac{1}{N_f} \int \frac{d^2 \mathbf{p}'_f}{(2\pi)^3 |\mathbf{v}'_f|} (\dots), \quad N_f = \int \frac{d^2 \mathbf{p}'_f}{(2\pi)^3 |\mathbf{v}'_f|}, \quad (10)$$

where  $N_f$  is the average density of states on the Fermi surface. The other material parameters that enter the self-consistency equations are the dimensionless pairing interaction,  $N_f V(\mathbf{p}_f, \mathbf{p}'_f)$ , the dimensionless Landau interaction,  $N_f A(\mathbf{p}_f, \mathbf{p}'_f)$ , the impurity concentration,  $n_i$ , the impurity potential,  $\check{u}(\mathbf{p}_f, \mathbf{p}'_f)$ , and the Fermi surface data:  $\mathbf{p}_f$  (Fermi surface),  $\mathbf{v}_f(\mathbf{p}_f)$  (Fermi velocity). We eliminate both the magnitude of the pairing interaction and the cut-off,  $\epsilon_c$ , in favor of the transition temperature,  $T_c$ , using the linearized, equilibrium form of the mean-field gap equation (Eq. (5)).

The quasiclassical equations are supplemented by constitutive equations for the charge density, the current density and the induced electromagnetic potentials. The formal result for the non-equilibrium charge density, to linear order in  $\Delta/E_f$ , is given in terms of the Keldysh propagator by

$$\rho^{(1)}(\mathbf{R}; t) = e N_f \int_{-\epsilon_c}^{+\epsilon_c} \frac{d\epsilon}{4\pi i} \langle Z(\mathbf{p}'_f) \text{Tr} [\hat{g}^K(\mathbf{p}'_f, \mathbf{R}; \epsilon, t)] \rangle - 2e^2 N_f Z_0 \Phi(\mathbf{R}; t), \quad (11)$$

with the renormalization factors given by

$$Z(\mathbf{p}_f) = 1 - \langle A(\mathbf{p}'_f, \mathbf{p}_f) \rangle, \quad Z_0 = \langle Z(\mathbf{p}_f) \rangle. \quad (12)$$

The high-energy renormalization factor is related to an average of the scattering amplitude on the Fermi surface by a Ward identity that follows from the conservation law for charge [14]. The charge current induced by  $\mathbf{A}(\mathbf{R}; t)$ , calculated to leading order in  $\Delta/E_f$ , is also obtained from the Keldysh propagator,

$$\mathbf{j}^{(1)}(\mathbf{R}; t) = eN_f \int \frac{d\epsilon}{4\pi i} \text{Tr} \langle \mathbf{v}_f(\mathbf{p}'_f) \hat{\tau}_3 \hat{g}^K(\mathbf{p}'_f, \mathbf{R}; \epsilon, t) \rangle. \quad (13)$$

There is no additional high-energy renormalization of the coupling to the vector potential because the quasiparticle Fermi velocity already includes the high-energy renormalization of the charge-current coupling in Eq. 13. Furthermore, the self-consistent solution of the quasiclassical equations for  $\hat{g}^K$  ensures the continuity equation for charge conservation,

$$\partial_t \rho^{(1)}(\mathbf{R}; t) + \nabla \cdot \mathbf{j}^{(1)}(\mathbf{R}; t) = 0, \quad (14)$$

is satisfied.

An estimate of the contribution to the charge density from the integral in Eq. (11) leads to the condition of “local charge neutrality” [17,18]. A charge density given by the elementary charge times the number of states within an energy interval  $\Delta$  around the Fermi surface implies  $\rho^{(1)} \sim 2eN_f\Delta$ . Such a charge density cannot be maintained within a coherence volume because of the cost in Coulomb energy. The Coulomb energy is suppressed by requiring the leading order contribution to the charge density vanish: i.e.  $\rho^{(1)}(\mathbf{R}; t) = 0$ . Thus, the spatially varying renormalized electro-chemical potential,  $Z_0\Phi$ , is determined by

$$2eZ_0\Phi(\mathbf{R}; t) = \int_{-\epsilon_c}^{+\epsilon_c} \frac{d\epsilon}{4\pi i} \text{Tr} \langle Z(\mathbf{p}'_f) \hat{g}^K(\mathbf{p}'_f, \mathbf{R}; \epsilon, t) \rangle. \quad (15)$$

The continuity equation implies  $\nabla \cdot \mathbf{j}^{(1)}(\mathbf{R}; t) = 0$ . We discuss violations of the charge neutrality condition (15), which are higher order in  $\Delta/E_f$ , in Sec. 4.1. Finally, Ampere’s equation, with the current given by Eq. (13), determines the vector potential in the quasiclassical approximation,

$$\nabla \times \nabla \times \mathbf{A}(\mathbf{R}; t) = \frac{8\pi e N_f}{c} \int \frac{d\epsilon}{4\pi i} \text{Tr} \langle \mathbf{v}_f(\mathbf{p}'_f) \hat{\tau}_3 \hat{g}^K(\mathbf{p}'_f, \mathbf{R}; \epsilon, t) \rangle. \quad (16)$$

Equations (2)-(9) and (15)-(16) constitute a complete set of equations for calculating the electromagnetic response of vortices in the quasiclassical limit. For high- $\kappa$  superconductors we can simplify the self-consistency calculations to some degree. Since quasiparticles couple to the vector potential via  $\frac{e}{c} \mathbf{v}_f \cdot \mathbf{A}$ , Eq. (16) shows that this quantity is of order  $8\pi e^2 N_f v_f^2 / c^2 = 1/\lambda^2$ , where  $\lambda$  is the magnetic penetration depth. Thus, for  $\kappa = \lambda/\xi_0 \gg 1$ , as in the layered cuprates, the feedback effect of the current density on the vector potential is small by factor  $1/\kappa^2$ .

## 2.2 Linear Response

For sufficiently weak fields we can calculate the electromagnetic response to linear order in the external field. The propagator and the self-energies are separated into unperturbed equilibrium parts and terms that are first-order in the perturbation,

$$\check{g} = \check{g}_0 + \delta\check{g}, \quad \check{\Delta}_{mf} = \check{\Delta}_0 + \delta\check{\Delta}_{mf}, \quad \check{\sigma}_i = \check{\sigma}_0 + \delta\check{\sigma}_i, \quad (17)$$

and similarly for the electromagnetic potentials,  $\mathbf{A} = \mathbf{A}_0 + \delta\mathbf{A}$ ,  $\Phi = \delta\Phi$ . The equilibrium propagators obey the matrix transport equation,

$$\left[ \left( \epsilon + \frac{e}{c} \mathbf{v}_f \cdot \mathbf{A}_0 \right) \check{\tau}_3 - \check{\Delta}_0 - \check{\sigma}_0, \check{g}_0 \right] + i \mathbf{v}_f \cdot \nabla \check{g}_0 = 0. \quad (18)$$

These equations are supplemented by the self-consistency equations for the mean fields, Eqs. (5)-(6), the impurity self energy, Eqs. (8)-(9), the local charge-neutrality condition for the scalar potential, Eq. (15), Ampère's equation for the vector potential, Eq. (16), the equilibrium normalization conditions,

$$\check{g}_0^2 = -\pi^2 \check{1}, \quad (19)$$

and the equilibrium relation between the Keldysh function and equilibrium spectral density,

$$\hat{g}_0^K = \tanh\left(\frac{\epsilon}{2T}\right) [\hat{g}_0^R - \hat{g}_0^A]. \quad (20)$$

The first-order correction to the matrix propagator obeys the linearized transport equation,

$$\left[ \left( \epsilon + \frac{e}{c} \mathbf{v}_f \cdot \mathbf{A}_0 \right) \check{\tau}_3 - \check{\Delta}_0 - \check{\sigma}_0, \delta\check{g} \right]_{\otimes} + i \mathbf{v}_f \cdot \nabla \delta\check{g} = [\delta\check{\Delta}_{mf} + \delta\check{\sigma}_i + \delta\check{v}, \check{g}_0]_{\otimes}, \quad (21)$$

with source terms on the right-hand side from both the external field ( $\delta\check{v}$ ) and the internal fields ( $\delta\check{\Delta}_{mf}$ ,  $\delta\check{\sigma}_i$ ). In addition, the first-order propagator satisfies the “orthogonality condition”,

$$\check{g}_0 \otimes \delta\check{g} + \delta\check{g} \otimes \check{g}_0 = 0. \quad (22)$$

obtained from linearizing the full normalization condition.<sup>2</sup> The system of linear equations are supplemented by the equilibrium and first-order self-consistency conditions for the order parameter,

$$\hat{\Delta}_0^{R,A}(\mathbf{p}_f, \mathbf{R}) = N_f \int_{-\epsilon_c}^{+\epsilon_c} \frac{d\epsilon}{4\pi i} \langle V(\mathbf{p}_f, \mathbf{p}'_f) \hat{f}_0^K(\mathbf{p}'_f, \mathbf{R}; \epsilon) \rangle, \quad (23)$$

$$\delta \hat{\Delta}_{mf}^{R,A}(\mathbf{p}_f, \mathbf{R}; t) = N_f \int_{-\epsilon_c}^{+\epsilon_c} \frac{d\epsilon}{4\pi i} \langle V(\mathbf{p}_f, \mathbf{p}'_f) \delta \hat{f}^K(\mathbf{p}'_f, \mathbf{R}; \epsilon, t) \rangle, \quad (24)$$

---

<sup>2</sup> Note that the convolution product between an equilibrium and a nonequilibrium quantity simplifies after Fourier transforming  $t \rightarrow \omega$ :  $\check{A}_0 \otimes \delta \check{B}(\epsilon, \omega) = \check{A}_0(\epsilon + \omega/2) \check{B}(\epsilon, \omega)$ ,  $\check{B}(\epsilon, \omega) \otimes \check{A}_0 = \check{B}(\epsilon, \omega) \check{A}_0(\epsilon - \omega/2)$ .

and the impurity self-energy,

$$\check{\sigma}_0(\mathbf{p}_f, \mathbf{R}; \epsilon) = n_i \check{t}_0(\mathbf{p}_f, \mathbf{p}_f, \mathbf{R}; \epsilon), \quad (25)$$

$$\check{t}_0(\mathbf{p}_f, \mathbf{p}_f'', \mathbf{R}; \epsilon) = \check{u}(\mathbf{p}_f, \mathbf{p}_f'') + N_f \langle \check{u}(\mathbf{p}_f, \mathbf{p}_f') \check{g}_0(\mathbf{p}_f', \mathbf{R}; \epsilon) \check{t}_0(\mathbf{p}_f', \mathbf{p}_f'', \mathbf{R}; \epsilon) \rangle, \quad (26)$$

$$\delta \check{\sigma}_i(\mathbf{p}_f, \mathbf{R}; \epsilon, t) = n_i N_f \langle \check{t}_0(\mathbf{p}_f, \mathbf{p}_f', \mathbf{R}; \epsilon) \otimes \delta \check{g}(\mathbf{p}_f', \mathbf{R}; \epsilon, t) \otimes \check{t}_0(\mathbf{p}_f', \mathbf{p}_f, \mathbf{R}; \epsilon) \rangle. \quad (27)$$

In general the diagonal mean fields also contribute to the response. However, we do not expect Landau interactions to lead to qualitatively new phenomena for the vortex dynamics, so we have neglected these interactions in the following analysis and set  $A(\mathbf{p}_f, \mathbf{p}_f') = 0$  (i.e.  $\check{\nu}_{mf} = 0$ ). As a result the local charge neutrality condition for the electro-chemical potential becomes,

$$2e\delta\Phi(\mathbf{R}; t) = \int_{-\epsilon_c}^{+\epsilon_c} \frac{d\epsilon}{4\pi i} \text{Tr} \langle \delta \hat{g}^K(\mathbf{p}_f, \mathbf{R}; \epsilon, t) \rangle. \quad (28)$$

In what follows we work in a gauge in which the induced electric field,  $\mathbf{E}^{\text{ind}}(\mathbf{R}; t)$ , is obtained from  $\delta\Phi(\mathbf{R}; t)$  and the uniform external electric field,  $\mathbf{E}_\omega^{\text{ext}}(t)$ , is determined by the vector potential  $\delta\mathbf{A}_\omega(t)$ . For  $\lambda/\xi_0 \gg 1$  we can safely neglect corrections to the vector potential due to the induced current. Thus, in the Nambu-Keldysh matrix notation the electromagnetic coupling to the quasiparticles is given by

$$\delta\check{v} = -\frac{e}{c} \mathbf{v}_f \cdot \delta\mathbf{A}_\omega(t) \check{\tau}_3 + e\delta\Phi(\mathbf{R}; t) \check{1}. \quad (29)$$

The validity of linear response theory requires the external perturbation  $\delta\check{v}$  be sufficiently small and that the induced vortex motion responds to the external field at the frequency set by the external field. At very low frequencies frictional damping of the vortex motion, arising from the finite mean free path of quasiparticles scattering from impurities, gives rise to a nonlinear regime in the dynamical response of a vortex. This regime is discussed extensively in the literature [13], and is not subject of our study. However, for sufficiently small field strengths the vortex motion is nonstationary over any time interval, although it may be regarded as quasi-stationary at low enough frequencies. The nonstationary motion of the vortex can be described by linear response theory if  $\delta\check{v} \ll 1/\tau$  for  $\omega \lesssim 1/\tau$ , and  $\delta\check{v} \ll \omega$  for  $\omega \gtrsim 1/\tau$ . Note that the frequency of the perturbation,  $\omega$ , is not required to be small compared to the gap frequency; it is only restricted to be small compared to atomic scale frequencies, e.g.  $\omega \ll E_f/\hbar$ .

Self-consistent solutions of Eqs. (24), (27) and (28) for the self-energies and scalar potential are fundamental to obtaining a physically sensible solution for the electromagnetic response. The dynamical self-energy corrections are equivalent to “vertex corrections” in the Kubo formulation of linear response theory. They are particularly important in the context of nonequilibrium phenomena in inhomogeneous superconductors.<sup>3</sup> In our case these corrections are of vital importance; the self-consistency conditions enforce charge conservation. In particular, Eqs. (25)-(27) imply charge conservation in scattering processes, whereas

<sup>3</sup> Vertex corrections usually vanish in homogeneous superconductors because of translational and rotational symmetries. Inhomogeneous states break these symmetries and typically generate non-vanishing vertex corrections.



(23) and (24) imply charge conservation in particle-hole conversion processes; any charge which is lost (gained) in a particle-hole conversion process is compensated by a corresponding gain (loss) of condensate charge. It is the coupled quasiparticle and condensate dynamics which conserves charge in superconductors. Neglecting the dynamics of either component, or using a non-conserving approximation for the coupling leads to unphysical results.

Self-consistent calculations for the equilibrium order parameter, impurity self-energy and local excitation spectrum (spectral density) are necessary inputs to the linearized transport equations for the dynamical response of a vortex. The equilibrium spectral function also provides key information for the interpretation of the dynamical response. Because of particle-hole coherence the spectral density is sensitive to the phase winding and symmetry of the order parameter, as well as material properties such as the transport mean-free path and impurity cross-section. In the following section we present results for the low-energy excitation spectra of singly- and doubly-quantized vortices in layered superconductors with *s*-wave and *d*-wave pairing symmetry.

### 3 Electronic Structure of Vortices

The local density of states for excitations with Fermi momentum  $\mathbf{p}_f$  is obtained from the retarded and advanced quasiclassical propagators,

$$N(\mathbf{p}_f, \mathbf{R}; \epsilon) = N_f \frac{1}{4\pi i} \text{Tr} [\hat{\tau}_3 \hat{g}_0^A(\mathbf{p}_f, \mathbf{R}; \epsilon) - \hat{\tau}_3 \hat{g}_0^R(\mathbf{p}_f, \mathbf{R}; \epsilon)] . \quad (30)$$

This function measures the local density of the quasiparticle states with energy  $\epsilon$  at the point  $\mathbf{p}_f$  on the Fermi surface. The local density of states (LDOS) is obtained by averaging this quantity over all momentum directions of the quasiparticles,

$$N(\mathbf{R}; \epsilon) = \langle N(\mathbf{p}'_f, \mathbf{R}; \epsilon) \rangle . \quad (31)$$

The product of the angle-resolved density of states and the Fermi velocity,  $\mathbf{v}_f$ , determines the current density carried by these states;  $\mathbf{v}_f$  also defines the direction of a quasiclassical trajectory passing through the space point  $\mathbf{R}$ . We introduce the angle-resolved *spectral current density* [3],

$$\mathbf{j}(\mathbf{p}_f, \mathbf{R}; \epsilon) = 2e\mathbf{v}_f(\mathbf{p}_f) N(\mathbf{p}_f, \mathbf{R}; \epsilon) , \quad (32)$$

which measures the current density carried by quasiparticle states with energy  $\epsilon$  moving along the trajectory defined by  $\mathbf{v}_f$ . The local spectral current density is then defined as

$$\mathbf{j}(\mathbf{R}; \epsilon) = \langle \mathbf{j}(\mathbf{p}'_f, \mathbf{R}; \epsilon) \rangle , \quad (33)$$

and the total current density is obtained by summing over the occupied states for each trajectory,

$$\mathbf{j}(\mathbf{R}) = \int d\epsilon f(\epsilon) \mathbf{j}(\mathbf{R}; \epsilon) , \quad (34)$$

where  $f(\epsilon) = 1/(1 + e^{\beta\epsilon})$ . Self-consistent calculations of the equilibrium structure and spectral properties of vortices are relatively straight-forward computations. Below we present results for  $s$ -wave and  $d$ -wave pairing symmetry with impurity scattering included.

The calculations reported are carried for a circular Fermi surface, with an isotropic Fermi momentum  $\mathbf{p}_f$  and Fermi velocity  $\mathbf{v}_f$ . The elastic scattering rate is chosen to represent the intermediate-clean regime,  $\Delta^2/E_f < \hbar/\tau \ll \Delta$ . The pairing potential can be represented as a sum over invariant products of basis functions  $\{\eta_{\Gamma,i}(\mathbf{p}_f)|i = 1 \dots d_\Gamma\}$  for the irreducible representations of the crystal point group labeled by  $\Gamma$ ,

$$N_f V(\mathbf{p}_f, \mathbf{p}'_f) = \sum_{\Gamma,i} v_\Gamma \eta_{\Gamma,i}^*(\mathbf{p}_f) \eta_{\Gamma,i}(\mathbf{p}'_f). \quad (35)$$

The pairing interaction,  $v_\Gamma$ , and the cutoff,  $\epsilon_c$ , are eliminated in favor of the instability temperature for pairing in symmetry channel  $\Gamma$ . We limit the discussion here to even-parity, one-dimensional representations, which for tetragonal symmetry includes the ‘ $s$ -wave’ (identity) representation,  $A_{1g}$ , two ‘ $d$ -wave’ representations,  $B_{1g}$  and  $B_{2g}$ , and a ‘ $g$ -wave’ representation,  $A_{2g}$ . The corresponding basis functions we use are listed in Table 1.

**Table 1.** Symmetry classes and model basis functions for the 1D even-parity representations of  $D_{4h}$ . The angle  $\phi$  is the angular position of  $\mathbf{p}_f$  on the Fermi surface with respect to the crystallographic  $a$ -axis ( $=x$ -axis).

Pairing Symmetry	Representation $[\Gamma]$	Basis Function $[\eta_\Gamma]$
$s$ -wave	$A_{1g}$	1
$d$ -wave	$B_{1g}$	$\sqrt{2} \cos(2\phi)$
$d'$ -wave	$B_{2g}$	$\sqrt{2} \sin(2\phi)$
$g$ -wave	$A_{2g}$	$\sqrt{2} \sin(4\phi)$

The results for the order parameter, impurity self energy and spectral properties of vortices that follow are calculated self consistently in the  $t$ -matrix approximation for point impurities (pure  $s$ -wave scattering), i.e.  $\tilde{u}(\mathbf{p}_f, \mathbf{p}'_f) = u_0 \hat{1}$ . The quasiparticle scattering rate,  $1/2\tau$ , and normalized impurity cross section,  $\bar{\sigma}$ , are then given by,

$$\frac{1}{2\tau} = \frac{n_i}{\pi N_f} \bar{\sigma}, \quad \bar{\sigma} = \frac{(\pi N_f u_0)^2}{1 + (\pi N_f u_0)^2}. \quad (36)$$

The Born limit corresponds to  $\bar{\sigma} \ll 1$ , while unitary scattering corresponds to  $|u_0| \rightarrow \infty$  or  $\bar{\sigma} \rightarrow 1$ . In the calculations that follow the temperature is set at  $T = 0.3T_c$ , and the mean free path is chosen to represent the intermediate-clean regime;  $\ell = 10 \xi_0$ .

### 3.1 Singly quantized vortices for S-wave Pairing

For isotropic  $s$ -wave pairing the equilibrium order parameter for an isolated vortex with winding number  $p$  has the form,

$$\Delta(\mathbf{p}_f, \mathbf{R}) = |\Delta(\mathbf{R})|e^{ip\varphi}, \quad (37)$$

where the amplitude  $|\Delta(\mathbf{R})|$  is isotropic and  $\varphi$  is the azimuthal angle of  $\mathbf{R}$  in the plane.

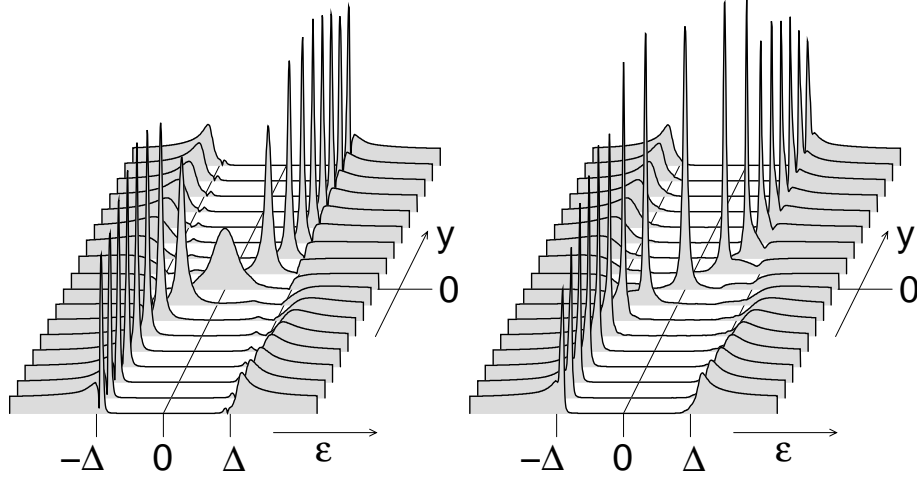


**Fig. 1.** Angle-resolved density of states for an  $s$ -wave vortex for quasiparticles propagating along trajectories parallel to the  $x$ -direction, at points along the  $y$ -axis spaced by  $1.38\xi_0$ . The left panel is for Born scattering, and the right panel is for unitary scattering with the same mean free path of  $\ell = 10\xi_0$ . The temperature is  $T = 0.3T_c$ .

The angle-resolved local density of states spectra for a singly quantized vortex is shown in Fig. 1 for space points  $\mathbf{R} = (0, y)$  along the  $y$ -axis with a spacing of  $\delta y = \sqrt{3}\pi/4\xi_0 \simeq 1.36\xi_0$ , and for trajectories parallel to the  $x$ -axis,  $\mathbf{v}_f = v_f \mathbf{e}_x$ . The vortex center is at  $y = 0$ , and the phase winding is such that the direction of the superflow is in  $x$ -direction for spectra with negative  $y$  coordinate.

Far outside the core the angle-resolved density of states resembles the BCS density of states with a gap in the spectrum roughly between  $\epsilon = \pm\Delta$ , and peaks in the spectrum near the continuum edges. Careful inspection of Fig. 1 shows that the coherence peak for positive energy at  $y = -8\delta y \simeq -11\xi_0$  is not at  $\epsilon = \Delta$ , but is shifted to higher energy by the Doppler effect,  $\Delta\epsilon = \mathbf{v}_f \cdot \mathbf{p}_s$ , where  $\mathbf{p}_s = \frac{1}{2}\hbar\nabla\vartheta - \frac{e}{c}\mathbf{A}$  is the condensate momentum [3]. In a homogeneous superflow field the spectrum is the Doppler-shifted BCS spectrum; the Doppler shift increases with condensate momentum until pairbreaking sets in at the bulk critical momentum,  $p_c = \Delta/v_f$ . However, in the vortex core *nonlocal effects* associated with the inhomogeneous flow field lead to a redistribution of the spectral weight

near the gap edge. The positive energy continuum edge is broadened considerably compared to the square-root singularity in the absence of the Doppler effect. The continuum starts at  $+\Delta$  even for the Doppler-shifted spectra near the maximal current regions. In contrast, the negative energy continuum edge shows sharp structures due to the accumulation of spectral weight in the region between  $-\Delta$  and  $-\Delta + \mathbf{v}_f \cdot \mathbf{p}_s$ . The sharp structure corresponds to a bound state that is separated from the continuum edge. The density of states at the continuum edge drops precipitously at  $\epsilon = -\Delta$ . We emphasize that nonlocal effects lead to qualitative differences in the spectrum near the gap edges compared to the widely used approximation of Doppler-shifted quasiparticles in a locally homogeneous superflow [19]. In clean superconductors nonlocal effects dominate the spectrum.

For a homogeneous superflow the current is carried mainly by the states that are Doppler shifted the region between  $-\Delta$  and  $\Delta$ . The spectral current density shows that contributions to the current density from states outside of this region nearly cancel. In the case of a vortex, the bound state that splits off from the continuum not only robs the Doppler-shifted continuum edge of its spectral weight, but the bound state also carries most of the supercurrent in the vortex core region. At distances approaching the vortex center the bound state is clearly resolved and disperses through  $\epsilon = 0$  at zero impact parameter. As shown in the left panel of Fig. 1 the bound state also broadens considerably for Born scattering as it disperses towards the Fermi level, but remains a sharp resonance in the limit of unitary scattering, as shown in Fig. 1.

The coherence peaks are completely suppressed at the vortex center, both in the Born and unitary limits. Note the difference in the evolution of the spectral weight for the bound and continuum states: for positive energies the spectral weight of the coherence peak is shifted to higher energies as one approaches the vortex core, with a continuously diminishing intensity at the coherence peak. In contrast, the spectral weight of the negative energy coherence peak is transferred to the bound state which splits off from the continuum. In principle there could be additional, secondary bound states, which would split off from the continuum if the vortex core were wider. However, a self-consistent calculation of the order parameter suppresses the secondary bound state in the vortex core. We return to the discussion of secondary bound states when we discuss the spectrum of pinned vortices. For trajectories with  $y > 0$  the structure of the spectrum for positive and negative energies is reversed because the superflow is now counter to the quasiparticle velocity, leading to negative Doppler shifts and bound states at positive energies below the continuum edge. The small spectral features that appear at the energies corresponding to the *negative* of the bound state energies are due to mixing of with trajectories of opposite velocity by backscattering from impurities.

Finally, consider the differences in the spectral features for unitary versus Born scattering. In Fig. 2 we show the local density of states at the center of the vortex for several scattering cross sections ranging from the Born limit ( $\bar{\sigma} \ll 1$ ) to the unitary limit ( $\bar{\sigma} = 1$ ). In the Born limit the broadening is a maximum.

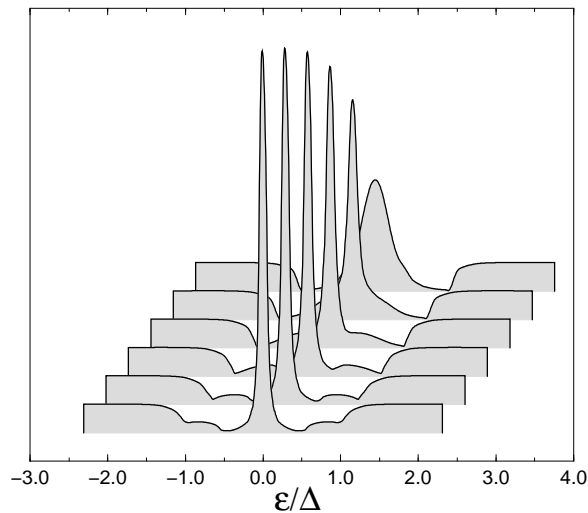


**Fig. 2.** Local density of states (LDOS) in the center of an  $s$ -wave vortex for different effective impurity scattering cross sections  $\bar{\sigma}$  from Born to unitary limit, with a fixed mean free path  $\ell = 10\xi_0$ , and temperature  $T = 0.3T_c$ . From top to bottom:  $\bar{\sigma} = 0.0, 0.2, 0.4, 0.6, 0.8, 1.0$ .

For small, but finite cross section two bands of impurity bound states split off from the zero-energy resonance and remove spectral weight from the central peak. The impurity bands evolve towards the continuum edges as the cross-section increases and merge with them in the unitary limit. When the impurity bound-state bands no longer overlap the central peak the zero-energy resonance sharpens dramatically with the width remaining constant as the unitary limit is approached. The overlap between the impurity bands and the continuum edges in the unitary limit is determined by the scattering rate, and is increasing with increasing scattering rate,  $1/\tau$ . As shown in the right panel of Fig. 1, the impurity bands are localized in the vortex core region; their existence depends on impurity scattering in a region where the phase changes rapidly over length scales of order the coherence length.

### 3.2 Singly quantized vortices for D-wave Pairing

For  $d$ -wave pairing symmetry the order parameter has the form,

$$\Delta(\mathbf{p}_f, \mathbf{R}) = \eta_{B_{1g}}(\mathbf{p}_f) \Delta(\mathbf{R}), \quad (38)$$

where  $\eta_{B_{1g}}(\mathbf{p}_f)$  changes sign on the Fermi surface at the points,  $\hat{\mathbf{p}}_{fx} = \pm \hat{\mathbf{p}}_{fy}$ . These nodal points lead to strong anisotropy and gapless excitations in the quasiparticle spectrum, which feeds back to produce anisotropy in the spatial structure of the order parameter in the core region of a vortex. The spatial

part of the order parameter,

$$\Delta(\mathbf{R}) = |\Delta(\mathbf{R})| e^{i\vartheta(\mathbf{R})}, \quad (39)$$

for a vortex, at distances far from the core, approaches that of an isotropic vortex:  $|\Delta(\mathbf{R})| \rightarrow \Delta(T)$  and  $\vartheta \rightarrow p\varphi$ . However, in the core region the current density is comparable to the critical current density and develops a four-fold anisotropy as a result of the backflow current concentrated near the nodes [20]. This current-induced pairbreaking effect is dominant for flow parallel to the nodal directions and leads to weak anisotropy of the order parameter in the core region.

The electronic structure of the  $d$ -wave vortex, presented in Fig. 3, shows distinct differences from that of an  $s$ -wave vortex. The resonances in the vortex core are broader than the core states of vortex in an  $s$ -wave superconductor. Mixing with extended states in nodal direction broadens the peaks near the continuum edges. Also note the effect of impurity scattering on the spectra far from the vortex core region, which show a broadened continuum rather than a sharp continuum edge. In the right panel of Fig. 3 we show the angle-resolved density of states for a  $d$ -wave vortex for unitary impurity scattering. As in the  $s$ -wave case there is sharpening of the zero resonance, but note that the width of the resonance is much broader than in the case of  $s$ -wave pairing because impurity scattering provides a coupling and mixing of the bound state resonance with the low-energy extended states for momenta near the nodal directions, even for a trajectory in the antinodal direction.

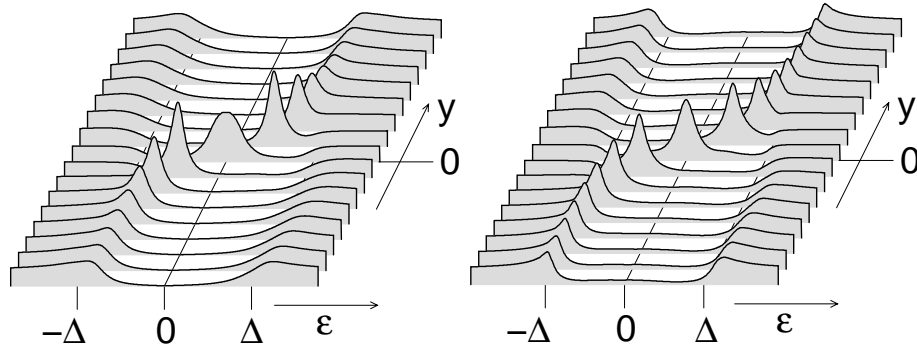


**Fig. 3.** Angle resolved density of states for a  $d$ -wave vortex for a quasiparticle trajectory along the  $x$ -direction (antinodal) as a function of impact parameter ( $y$ -direction). The impact parameter spacing is  $\delta y = 1.36\xi_0$ . The left panel corresponds to impurity scattering in the Born limit, and the right panel is for the unitary limit. The temperature is  $T = 0.3T_c$ .

In Fig. 4 we show the local density of states (LDOS) for both  $s$ -wave (top two panels) and  $d$ -wave pairing (bottom two panels) as a function of position  $\mathbf{R}$  along an anti-nodal direction (bottom left) and along a nodal direction (bottom right). The LDOS is obtained by averaging the angle-resolved density of states

over the Fermi surface at a particular space point  $\mathbf{R}$ . The averaging, together with the dispersion of the bound states and resonances as a function of angle leads to one-dimensional bands with characteristic Van Hove singularities, which are clearly visible for  $s$ -wave symmetry, but considerably smeared and broadened for  $d$ -wave symmetry. The LDOS for a vortex with  $s$ -wave pairing symmetry is shown for impurity scattering in both the Born (top left) and unitary limits (top right). The spectra show the characteristic bound state bands, Van Hove singularities and the dramatic reduction in the width of the zero bias resonance for unitary scattering.

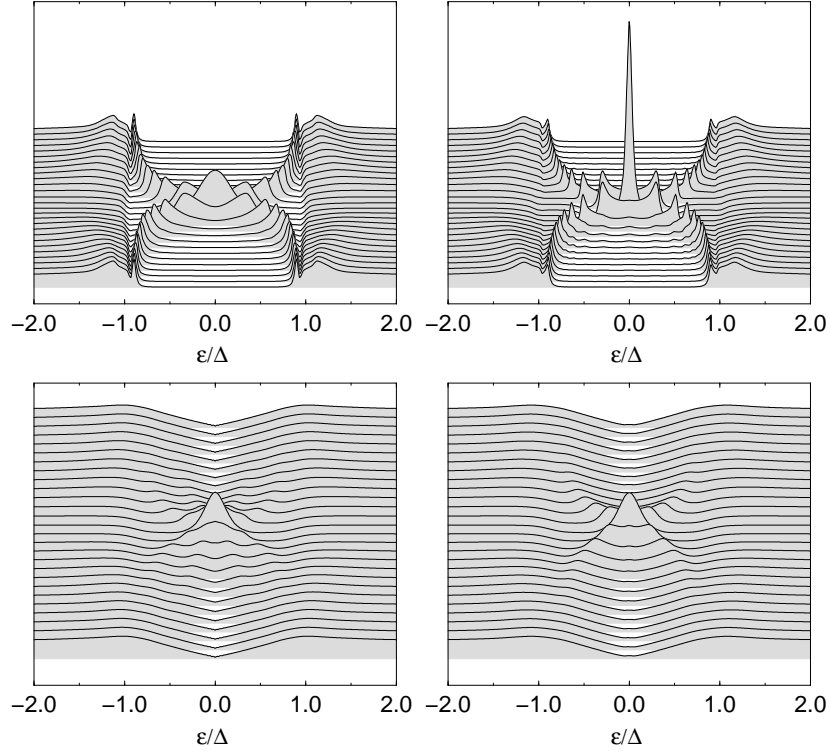


**Fig. 4.** Local density of states for an  $s$ -wave vortex (top panels) and a  $d$ -wave vortex (bottom panels), as a function of distance from the vortex center with a spacing  $\delta y = 0.79\xi_0$ . For  $s$ -wave pairing the Born limit is shown on the left and unitary scattering is on the right. For  $d$ -wave pairing the LDOS is shown only for Born scattering, but along axes parallel to a anti-nodal direction (left) and parallel to the nodal (right). The temperature is  $T = 0.3T_c$ .

Calculations of the LDOS in the superclean limit for a vortex with  $d$ -wave pairing are discussed by Schopohl and Maki [21] and by Ichioka *et al.* [22]. The self-consistent calculations shown in Fig. 4 include impurity scattering in the

Born limit for space points,  $\mathbf{R}$ , along two different directions; the left panel corresponds the LDOS measured as a function of distance along the anti-nodal direction and the right panel is the LDOS measured along the nodal direction. The nodes of the order parameter for  $d$ -wave pairing lead to continuum states with energies down to the Fermi level. These states are visible in the LDOS as the smooth background extending to zero energy from both positive and negative energies, even for distances far from the core. In the vortex core region several broad peaks disperse as a function of distance from the vortex center. These peaks correspond to broadened Van Hove singularities resulting from averaging the vortex core resonances over the Fermi surface for at a fixed position  $\mathbf{R}$ . The differences in the  $d$ -wave spectra for the two directions reflects the weak fourfold anisotropy of the LDOS around the vortex at fixed energy.

### 3.3 Vortices pinned to mesoscopic metallic inclusions

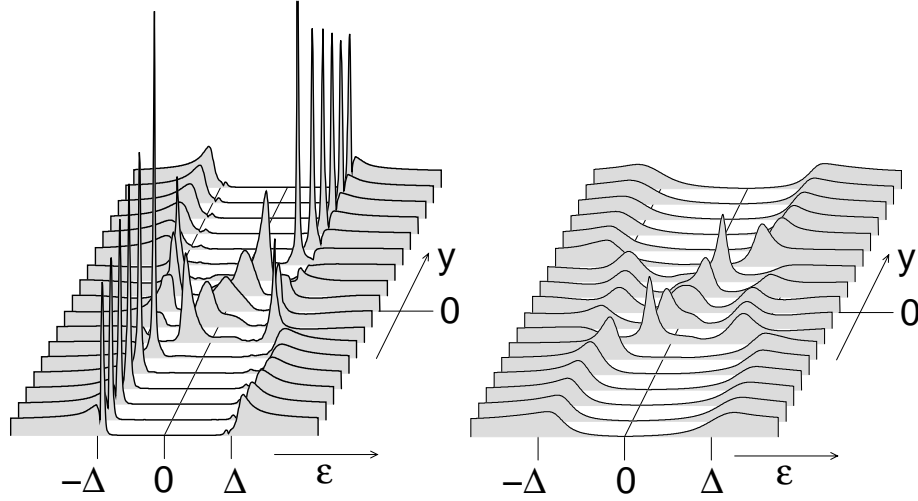
The calculations discussed above describe the average effects of atomic scale impurity disorder on the spectral properties of a vortex. A specific defect can also act as a pinning site for a vortex. We model such a defect as a mesoscopic size, normal metallic inclusion in the superconductor. The defect is assumed to be a circular inclusion, with a radius,  $\xi_{\text{pin}}$ , of order the coherence length of the superconductor. For simplicity we assume that the metallic properties of the inclusion, e.g. Fermi surface parameters, are the same as those of the normal-state of the host superconductor. The calculations presented below neglect normal reflection processes at the interface between the inclusion and the host metal, but include Andreev reflection. The analysis and calculations can be generalized for more detailed models of a pinning center.

Figures 5 and 6 show the angle-resolved local density of states and the LDOS for a vortex pinned on a metallic inclusion of radius  $\xi_{\text{pin}} = \pi\xi_0$ . The order parameter, impurity self energy and spectral densities were calculated self consistently for impurity scattering in the Born limit. Qualitative changes resulting from the inclusion occur inside the pinning center. The shape of the bound state resonance lines are asymmetric in energy. The asymmetry arises from multiple Andreev reflection processes by the interface between the pinning center and the superconductor, which leads to additional bands of resonances that overlap the vortex core resonances.

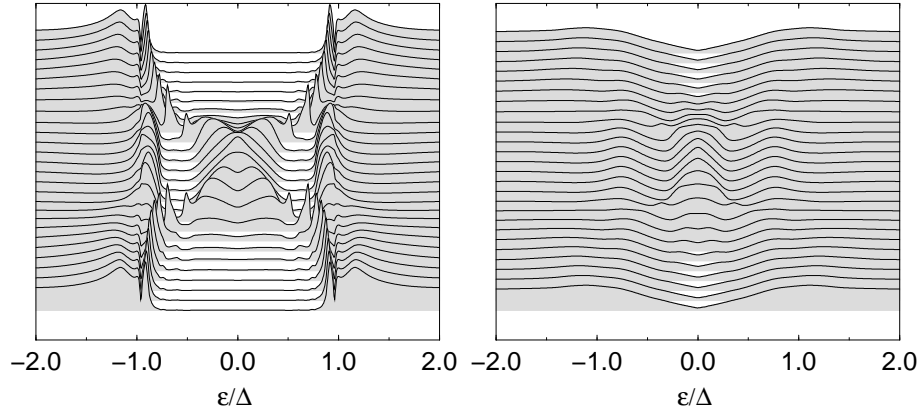
In addition to the asymmetry in the linewidth of the resonances the zero-energy bound state at the vortex center has a peculiar spectral shape, shown in more detail in Fig. 7 for  $s$ -wave pairing symmetry, but also visible in the right panel of Fig. 6 for  $d$ -wave pairing symmetry as well. In contrast to the spectra for a vortex without a pinning center, the coherence peaks at the continuum edges are present at the vortex center.

Figure 7 shows the peaks near the continuum edges in the vortex center for a pinned vortex. The spectral weight near the continuum edge is taken from the resonance at the Fermi level. The enhanced weight at the continuum edges is a precursor to the formation of a secondary bound state that splits off from the continuum. This can be seen in the evolution of the spectral density at





**Fig. 5.** Angle resolved density of states for a quasiparticle trajectory along the  $x$ -direction, as a function of impact parameter ( $y$ -axis) with a spacing of  $\delta y = 1.36\xi_0$  for a vortex centered on a pinning center of radius of  $\xi_{\text{pin}} = \pi\xi_0$ . The left panel is for  $s$ -wave symmetry and right panel is for  $d$ -wave symmetry. Impurity scattering is included for Born scattering with  $\ell = 10\xi_0$ . The temperature is  $T = 0.3T_c$ .



**Fig. 6.** Local density of states as a function of distance from the vortex center, with a spacing of  $\delta y = 0.79\xi_0$ , for a vortex pinned to an inclusion of radius of  $\xi_p = \pi\xi_0$ . The left panel corresponds to  $s$ -wave symmetry and the right panel is for  $d$ -wave symmetry along the anti-nodal direction. The temperature is  $T = 0.3T_c$ .

the vortex center as a function of the radius of the pinning center. There is a zero energy resonance for all pinning radii, however, increasing the radius of the pinning center transfers spectral weight from the zero-energy resonance to the continuum edge. A coherence peak develops, splits off from the continuum edge, strengthens and evolves to energies within the gap as the pinning radius changes from  $\xi_{\text{pin}} = 0.79\xi_0$  to  $\xi_{\text{pin}} = 4.71\xi_0$ . Thus, the appearance of the coherence peak for pinning centers the size of a coherence length or so is a precursor to the formation of a secondary bound state within the gap. The spectral weight comes at the expense of states just above the continuum edge and the zero-energy bound state, which is diminished in intensity with increasing pinning radius.

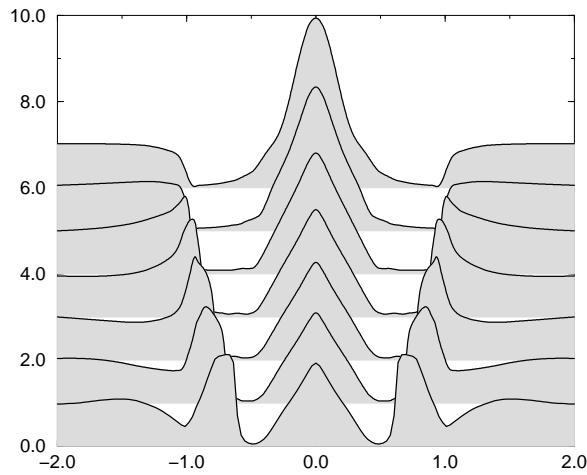


**Fig. 7.** Local density of states at the center of a vortex pinned in the center of a normal inclusion. The spectra (from top to bottom) correspond to different pinning radii:  $\xi_{\text{pin}} = 0, 0.79\xi_0, 1.57\xi_0, 2.36\xi_0, 3.14\xi_0, 3.93\xi_0$ , and  $4.71\xi_0$ . The temperature is  $T = 0.3T_c$ .

### 3.4 Doubly quantized vortices

Vortices with winding numbers larger than  $p = 1$  generally have line energies per unit winding number that are larger than that of a singly quantized vortex.<sup>4</sup> Nevertheless, doubly quantized vortices once formed are metastable and in principle it should be possible to observe the rare doubly quantized vortex using an atomic probe such as a scanning tunneling microscopic [25,26]. The spectrum of a doubly quantized vortex differs in a fundamental way from that

<sup>4</sup> There are counter examples for unconventional pairing with a multi-component order parameter in which the lowest energy vortex states are doubly quantized vortices [23,24].

of a singly quantized vortex. The singly quantized vortex, has a single branch of states that disperse through zero energy at the vortex center. The zero mode is guaranteed in the quasiclassical limit by  $\pi$  change along trajectories that pass through the vortex center. In contrast, there is no phase change along a trajectory through the vortex center for a doubly quantized vortex, and thus no topological requirement enforcing a zero energy bound state at the center of a doubly quantized vortex. Nevertheless, there is a spectrum of bound states in the cores of doubly quantized vortices which lead to characteristic structures in the LDOS and current spectral density of a doubly quantized vortex.

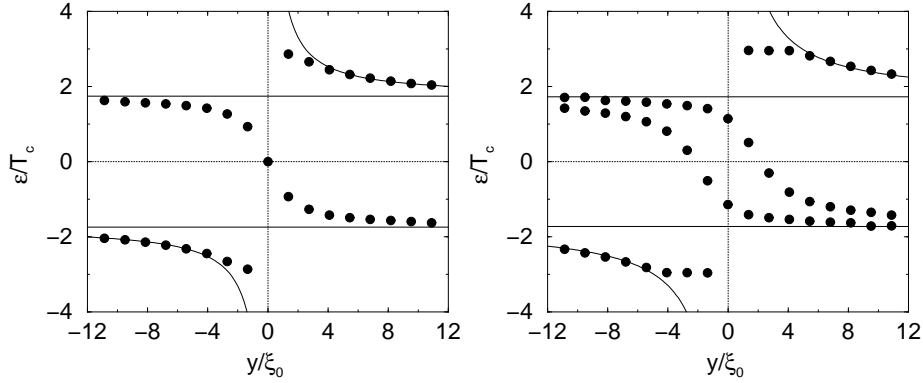


**Fig. 8.** Dispersion of the bound states (below the continuum edge) and of the coherence peaks (above the continuum edge) for quasiparticle trajectories in  $x$  direction as a function of  $y$ , for a singly quantized vortex (left) and for a doubly quantized vortex (right). The center of the vortex is at  $y = 0$ . Born impurity scattering with a mean free path of  $\ell = 10\xi_0$  is assumed. The temperature is  $T = 0.3T_c$ . The thin lines show the energies of the continuum edges and the Doppler shifted energies of the coherence peaks, assuming the London form for the condensate momentum  $\mathbf{p}_s = p\mathbf{e}_\phi/2r$ , where  $p$  is the winding number. The dispersion is shown for  $s$ -wave pairing; the corresponding data for  $d$ -wave pairing is similar.

This structure was discussed for a doubly quantized vortex in the superclean limit in Ref. [3]. Figure 9 shows the angle-resolved density of states for a doubly quantized vortex in an  $s$ -wave superconductor for trajectories parallel to the  $x$ -axis at different impact parameters along the  $y$ -direction. Two branches of vortex bound states cross the Fermi level at distances of order a coherence length from the vortex center. Thus, zero-energy bound states exist in the core but they are localized (for  $s$ -wave pairing symmetry) on trajectories at finite impact parameter from the vortex center. The locus of these trajectories forms a circle of radius  $r_{bs} \simeq 2.5\xi_0$  around the vortex center. Also note that the Doppler shift of the continuum spectrum is twice that for singly quantized vortices.

This can be seen by comparing the spectra far from the core in Figs. 9 and 1. The distinctive features in the spectrum of a doubly quantized vortex are

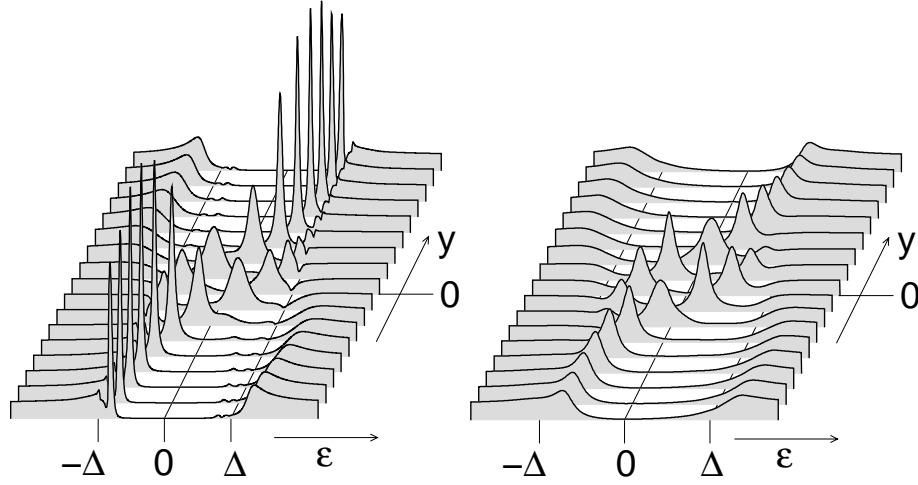


**Fig. 9.** Angle resolved density of states for a doubly quantized vortex along quasiparticle trajectories parallel to the  $x$ -direction, as a function of impact parameter,  $y$ , with a spacing  $\delta y = 1.36\xi_0$ . The left panel corresponds to  $s$ -wave symmetry and the right panel is for  $d$ -wave symmetry. Impurity scattering is included self-consistently in the Born limit with a mean free path  $\ell = 10\xi_0$ . The temperature is  $T = 0.3T_c$ .

present for either  $s$ - and  $d$ -wave pairing symmetry. The doubling of bound state branches that cross the Fermi level is observed for both pairing symmetries. The main difference in the spectra, as in the case of singly quantized vortices, is in the width of the resonances.

The most distinguishing feature of doubly quantized vortices is that the supercurrents near the center of the vortex flow *counter* to the asymptotic superflow associated with the phase winding around the vortex [3]. The counter circulating currents in the core, shown in the right panel of Fig. 11, are due to the bound states interior to the radius defined by the zero-energy bound state (Note that the zero-energy bound state itself does not carry current). This structure is revealed in Figs. 10 and 11, which show the LDOS and spectral current density for a doubly quantized vortex with  $s$ -wave and  $d$ -wave pairing symmetry. The left panel of Fig. 11 also shows the cumulative spectral current density and the reversal of the current for as one branch of bound states disperses below the Fermi level for  $r < r_{bs}$ .

These spectra show that the current density near the vortex core is carried mainly by the bound states, and that the reversal of the current direction near the vortex center is due to the branch of counter-flowing bound states dispersing below the Fermi level for impact parameter  $r < r_{bs}$ . In this region of the core the co-moving bound state is above the Fermi level so the asymmetry in the level occupation produces a counter flowing current.

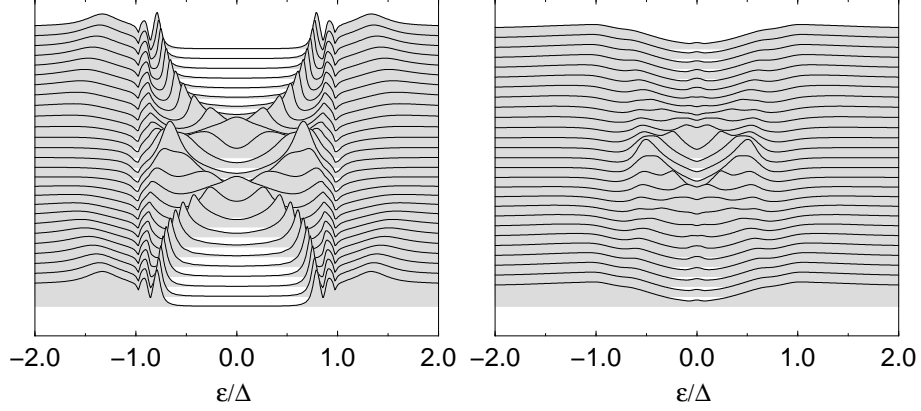


**Fig. 10.** Local density of states for doubly quantized vortices along trajectories parallel to the  $x$ -axis as a function of impact parameter along the  $y$ -axis with a spacing of  $\delta y = 1.36\xi_0$ . The left panel corresponds to  $s$ -wave pairing symmetry, and the right panel is for  $d$ -wave pairing along the anti-nodal direction. Impurity scattering is included in the Born limit with a mean free path of  $\ell = 10\xi_0$  and the temperature is  $T = 0.3T_c$ .

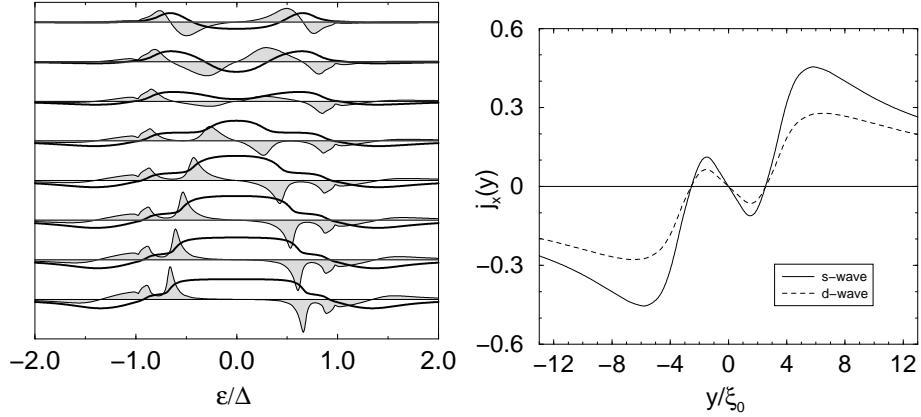


**Fig. 11.** The spectral current density for a doubly quantized vortex is shown along a trajectory parallel to the  $x$ -axis as a function of impact parameter ( $y$ -axis) with a spacing  $\delta y = 1.36\xi_0$ , starting at  $y = 1.36\xi_0$ . The thick curve is the cumulative spectral current density as a function of  $\epsilon$ , obtained by integrating  $j_x(\epsilon; y)$  from  $-\infty$  to  $\epsilon$ . The right panel is the  $x$ -component of the current density as a function of impact parameter for  $s$ -wave (solid line) and  $d$ -wave (dashed line) pairing.

## 4 Nonequilibrium Response

The dynamics of the electronic excitations of the vortex core play a key role in the dissipative processes in type II superconductors. Except in the dirty limit,  $\ell \ll \xi_0$ , the response of the core states to an electromagnetic field is generally very different from that of normal electrons. It is energetically unfavorable to maintain a charge density of the order of an elementary charge over a region with diameter of order the coherence length. Instead an electrochemical potential is induced which ensures that almost no net charge accumulates in the core region. However, a dipolar-like charge distribution develops which generates an internal electric field in the core. The internal field varies on the scale of the coherence length. This leads to a nonlocal response of the quasiparticles to the total electric field, even when the applied field varies on a much longer length scale and can be considered to be homogeneous. The dynamical response of the vortex core includes the collective mode of the inhomogeneous order parameter. This mode couples to the electro-chemical potential,  $\delta\Phi$ , in the vortex core region. This potential is generated by the charge dynamics of vortex core states and gives rise to internal electric fields which in turn drive the current density and the order parameter near the vortex core region. The induced electric fields in the core are the same order of magnitude as the external field. The dynamics of the core states are strongly coupled to the charge current and collective mode of the order parameter. Thus, the determination of the induced order parameter, as well as the spectrum and distribution function for the core states and nonequilibrium impurity scattering processes requires dynamical self consistency. Numerous calculations of the a.c. response neglect the self-consistent coupling of the collective mode and the spectral dynamics, or concentrate on the  $\omega \rightarrow 0$  limit [27,28,29,30]. Quasiclassical theory is the only formulation of the theory of nonequilibrium superconductivity presently capable of describing the nonlocal response of the order parameter and quasiparticle dynamics in the presence of mesoscopic inhomogeneities and disorder. The numerical solution to the self-consistency problem was presented for unpinned vortices in Ref. [31]. Here we report results for the electromagnetic response of isolated vortices bound to a pinning center in a superconductor with  $s$ -wave pairing symmetry.

### 4.1 Dynamical charge response

The charge dynamics of layered superconductors has two distinct origins. The  $c$ -axis dynamics is determined by the Josephson coupling between the conducting planes. Here we are concerned with the in-plane electrodynamics associated with the response of the order parameter and quasiparticle states bound to the vortex core. We assume strong Josephson coupling between different layers, and neglect variations of the response between different layers. This requires that the polarization of the electric field be in-plane, so that there is no coupling of the in-plane dynamics to the Josephson plasma modes. The external electromagnetic field is assumed to be long wavelength compared to the size of the vortex core,  $\lambda_{\text{EM}} \gg \xi_0$ . In this limit we can assume the a.c. electric field to be uniform

and described by a vector potential,  $\mathbf{E}_\omega(t) = -\frac{1}{c}\partial_t\mathbf{A}_\omega$ . We can also neglect the response to the a.c. magnetic field in the limit  $\lambda \gg \xi_0$ . In this case the spatial variation of the induced electric field occurs mainly within each conducting layer on the scale of the coherence length,  $\xi_0$ . Poisson's equation implies that induced charge densities are of order  $\delta\Phi/\xi_0^2$ , where  $\delta\Phi$  is the induced electrochemical potential in the core. This leads to a dynamical charge of order  $e(\Delta/E_f)$  in the vortex core. Once the electrochemical potential is calculated from Eq. (28) we can calculate the charge density fluctuations of order  $(\Delta/E_f)^3$  from Poisson's equation,

$$\rho^{(3)}(\mathbf{R};t) = -\frac{1}{4\pi}\nabla^2\Phi(\mathbf{R};t). \quad (40)$$

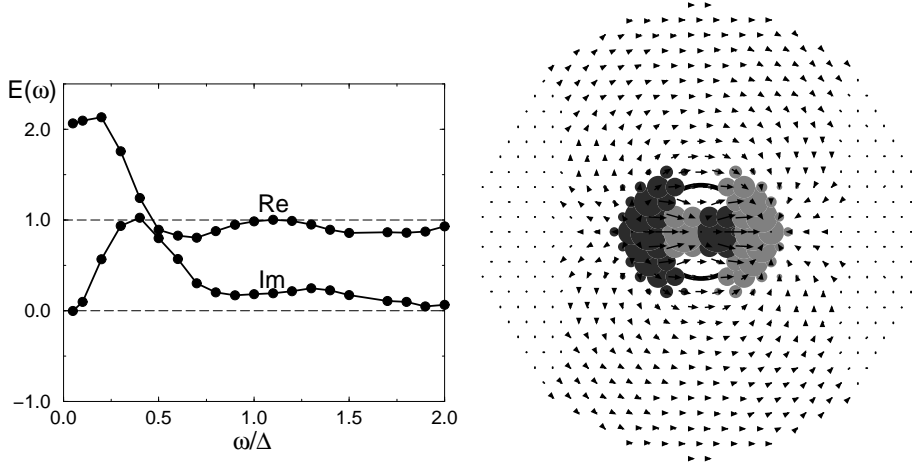


**Fig. 12.** Left: Total electric field in the center of a pinned  $s$ -wave vortex as a function of frequency  $\omega$  of an external a.c. electric field with polarization vector in the  $x$ -direction and wavelength large compared to  $\xi_0$ . Right: The corresponding in phase charge response around the pinning site for frequency  $\omega = 0.1\Delta$ . Gray corresponds to negative charge and black to positive charge. The arrows denote the total electric field vectors. The pinning center is a circular normal metallic inclusion with a radius  $\xi_p = 1.57\xi_0$ , shown as the black circle. Impurity scattering is included in the Born limit with a mean free path of  $\ell = 10\xi_0$ . The temperature is  $T = 0.3T_c$  and the calculations are carried out in the high- $\kappa$  limit.

In Fig. 12 we show the total electric field (external plus induced) acting on the quasiparticles in units of the external field. For  $\omega \gtrsim 2\Delta$  the total field is approximately equal to the external field. However, at frequencies  $\omega < 2\Delta$  an out-of-phase response develops. For  $\omega \ll \Delta$ , the total field in the pinning region approaches twice the external field, and the out-of-phase component vanishes. In the intermediate frequency region,  $0.1\Delta \lesssim \omega \lesssim \Delta$ , both in-phase and out-of-phase components are comparable. The right panel of Fig. 12 shows the charge

distribution for  $\omega = 0.1\Delta$  which oscillates out of phase with the external field. A dipolar charge distribution accumulates at the interface between the superconductor and the normal inclusion, oscillating at the frequency of the external field. At the center of the pinning site the out-of-phase component of the field is nearly zero at low frequencies (see also the left panel). The induced charge which accumulates is of order of  $e\Delta/E_f$  within a region of order  $\xi_0^2$  in each conducting layer. This charge is a factor of  $E_f/\Delta$  larger than the static charge of a vortex that arises from particle-hole asymmetry [32,33,34].

## 4.2 Local Dynamical Conductivity

Because the total electric field varies on the scale of a coherence length, the current response expressed in terms of the the total field is nonlocal in the intermediate clean regime. However, we can define a local conductivity tensor in terms of the response to the external field, provided the external field varies on a length scale large compared to the coherence length,

$$J_\mu(\mathbf{R}, \omega) = \sigma_{\mu\nu}(\mathbf{R}, \omega) E_\nu^{\text{ext}}(\omega). \quad (41)$$

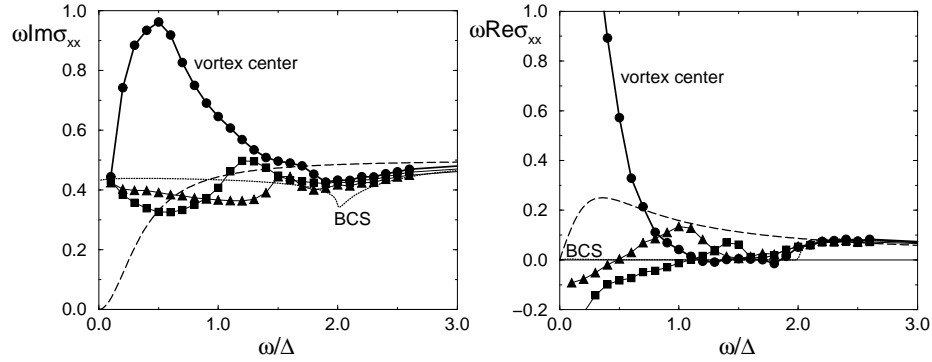


**Fig. 13.** Imaginary (left) and real part (right) of the local conductivity (multiplied with  $\omega$  for convenience) in the center of an unpinned  $s$ -wave vortex (circles), and at different distances from the center along the  $y$ -axis:  $1.1\xi_0$  (squares), and  $2.2\xi_0$  (triangles), as a function of frequency  $\omega$  of an external a.c. electric field with polarization vector in  $x$ -direction and wavelength large compared to  $\xi_0$ . Impurity scattering is taken into account in Born limit with a mean free path of  $\ell = 10\xi_0$ . The temperature is  $T = 0.3T_c$ . Calculations are done in the high- $\kappa$  limit. Also shown are the response for a homogeneous  $s$ -wave superconductor (dotted, denoted ‘BCS’), and the Drude conductivity of the normal metal (dashed).

Figures 13 and 14 show results for the conductivity,  $\sigma_{||}$ , in the vortex core region as a function of frequency for both unpinned and pinned vortices. For the pinned vortex the radius of the pinning center is  $\xi_{\text{pin}} = 1.57\xi_0$ .



First consider the unpinned vortex. The absorptive part of the conductivity (right panel of Fig. 13) is strongly enhanced at the vortex center compared to the normal-state Drude conductivity. The reactive response exhibits a maximum at a frequency determined by the impurity scattering rate. A few coherence lengths away from the vortex center the real part of the conductivity changes sign at low frequencies. This is a signature that energy is transported by vortex-core excitations away from the vortex center producing “hot spots” outside the core. The net dissipation is determined by inelastic scattering processes in the region around the vortex core. At distances of order a coherence length or so from the vortex center there is also structure in the conductivity spectrum at higher frequencies reflecting absorptive transitions between quasiparticle excitations with energies corresponding to the Van Hove singularities in the local density of states. The maxima in the absorptive part of the conductivity at  $y = 1.36\xi_0$  and  $2.72\xi_0$  from the center correspond to the energy level separation between the Van Hove peaks above and below the Fermi level shown in Fig. 4.

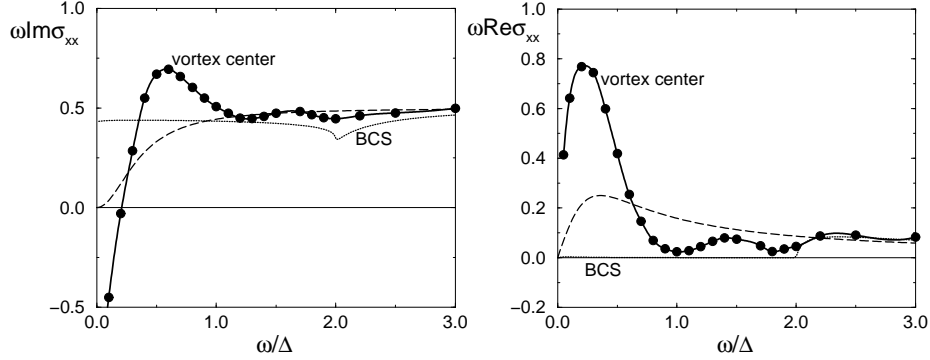


**Fig. 14.** Like Fig. 13 for a pinned vortex with a pinning radius  $\xi_p = 1.57\xi_0$ . As pinning site a circular normal conducting inclusion located at the center of the vortex was assumed (see Fig. 12).

The conductivity spectra for a vortex pinned by a metallic inclusion at its center is shown in Fig. 14. The most significant difference compared to the unpinned vortex occurs at frequencies  $\omega < 1/\tau$ . The absorptive part of the conductivity (right panel) is reduced compared to that of the unpinned case at low frequencies. The three broad peaks in the absorption spectrum correspond to scattering and dissipation within the zero-energy resonance (the dominant low-frequency peak), transitions between the zero-energy resonance and the continuum (the peak near  $\omega \sim 1.5\Delta$ ), and pair-breaking transitions from the negative energy to positive energy continuum states (broad peak above  $2\Delta$ ). The other notable feature is the reactive response at low frequencies which becomes *negative* in the low frequency limit, corresponding to superflow in the core that is counter to the induced supercurrent outside the vortex core and pinning center. This counter-

flow is required in order to satisfy the conductivity sum rule. The counterflow in the vortex center is also present for unpinned vortices, but at smaller frequencies for this particular impurity scattering rate. The low-frequency counterflow is also related to characteristic current patterns associated with low-frequency vortex dynamics which we discuss below.

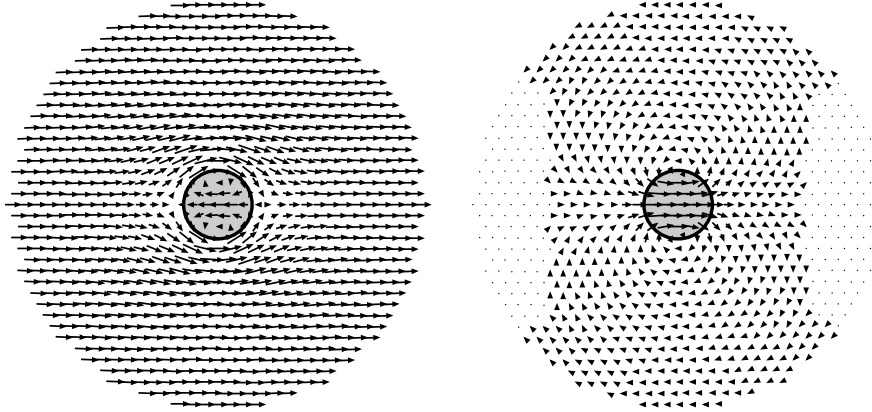


**Fig. 15.** *a.c.* current density pattern for an pinned *s*-wave vortex with a pinning radius  $\xi_p = 1.57\xi_0$ . As pinning site a circular normal conducting inclusion located at the center of the vortex was assumed. The border of the pinning center (gray) is shown as black circle. The frequency of the external electric field with polarization vector in *x*-direction is chosen  $\omega = 0.1\Delta$ . Left picture for out of phase (reactive) response, right picture for in phase (absorptive) response. Impurity scattering is taken into account in Born limit with a mean free path of  $\ell = 10\xi_0$ . The temperature is  $T = 0.3T_c$ . Calculations are done in the high- $\kappa$  limit.

### 4.3 Induced current density

Results for the *a.c.* component of the current density near a pinned vortex are shown in Fig. 15 for  $\omega = 0.1\Delta$ . In addition to the *a.c.* current there is the time-independent circulating supercurrent around the vortex center which adds to the current shown in Fig. 15. The current response shows a dipolar pattern, which is also observed for unpinned vortices. The in-phase current response (right panel) indicates a region of strong absorption within the pinning region ( $\mathbf{j} \parallel \mathbf{E}^{\text{ext}}$ ), and emission ( $\mathbf{j} \cdot \mathbf{E}^{\text{ext}} < 0$ ) in the region roughly perpendicular to the direction of the applied field several coherence lengths away from the pinning center. Calculations of the energy transport current show that energy absorbed in the core is transported away from the vortex center by the vortex core excitations in directions predominantly perpendicular to the applied field. The net absorption is ultimately determined by inelastic scattering and requires integrating the local

absorption and emission rate over the vortex array. Note that the long-range dipolar component does not contribute to the total dissipation. Far from the vortex core the current response is out of phase with the electric field and predominantly a non-dissipative supercurrent. Also note that at low frequency we clearly observe the counterflowing supercurrent within the pinning center.

#### 4.4 Summary

The electrodynamics of the vortex state in the intermediate-clean regime is non-local and largely determined by the response of the vortex-core states. Transitions involving the vortex-core states, and their coupling to the collective motion of the condensate requires dynamically self-consistent calculations of the order parameter, self energies, induced fields, excitation spectra and distribution functions. The results of these calculations provide new insight into the dynamics of vortex cores in conventional and unconventional superconductors.

#### 4.5 Acknowledgement

This work was supported in part by the NSF through grant DMR-9972087.

## References

1. C. Caroli, P. G. deGennes, and J. Matricon, Phys. Lett. **9**, 307 (1964).
2. J. Bardeen, R. Kümmel, A. E. Jacobs, and L. Tewordt, Phys. Rev. **187**, 556 (1969).
3. D. Rainer, J. A. Sauls, and D. Waxman, Phys. Rev. B **54**, 10094 (1996).
4. J. Bardeen and M. J. Stephen, Phys. Rev. **140**, A1197 (1965).
5. A. I. Larkin and Y. N. Ovchinnikov, Phys. Rev. B **57**, 5457 (1998).
6. A. A. Koulakov and A. I. Larkin, Phys. Rev. B **59**, 12021 (1999).
7. W. A. Atkinson and A. H. MacDonald, Phys. Rev. B **60**, 9295 (1999).
8. N. B. Kopnin and G. E. Volovik, Phys. Rev. Lett. **79**, 1377 (1997).
9. G. Eilenberger, Zeit.f. Physik **214**, 195 (1968).
10. A. I. Larkin and Y. N. Ovchinnikov, Sov. Phys. JETP **28**, 1200 (1969).
11. G. M. Eliashberg, Sov. Phys. JETP **34**, 668 (1972), [zetf, 61, 1254 (1971)].
12. A. Larkin and Y. Ovchinnikov, Sov. Phys. JETP **41**, 960 (1976).
13. A. Larkin and Y. Ovchinnikov, Sov. Phys. JETP **46**, 155 (1977).
14. J. W. Serene and D. Rainer, Phys. Rep. **101**, 221 (1983).
15. A. I. Larkin and Y. N. Ovchinnikov, in *Modern Problems in Condensed Matter Physics*, edited by D. Langenberg and A. Larkin (Elsevier Science Publishers, Amsterdam, 1986).
16. D. Rainer and J. A. Sauls, in *Superconductivity: From Basic Physics to New Developments*, edited by P. N. Butcher and Y. Lu (World Scientific, Singapore, 1995), pp. 45–78.
17. L. Gorkov and N. Kopnin, Sov. Phys. -Usp. **18**, 496 (1976).
18. S. Artemenko and A. Volkov, Sov. Phys. -Usp. **22**, 295 (1979).
19. M. Franz and Z. Tesanovic, Phys. Rev. B **60**, 3581 (1999).
20. S. K. Yip and J. A. Sauls, Phys. Rev. Lett. **69**, 2264 (1992).
21. N. Schopohl and K. Maki, Phys. Rev. B **52**, 490 (1995).

22. M. Ichioka, N. Hayashi, N. Enomoto, and K. Machida, Phys. Rev. B **53**, 15316 (1996).
23. T. Tokuyasu, D. Hess, and J. A. Sauls, Phys. Rev. B **41**, 8891 (1990).
24. A. S. Mel'nikov, Sov. Phys. JETP **74**, 1059 (1992).
25. H. Hess *et al.*, Phys. Rev. Lett. **62**, 214 (1989).
26. C. Renner, A. D. Kent, P. Niedermann, and Ø. Fischer, Phys. Rev. Lett. **70**, 3135 (1991).
27. B. Janko and J. Shore, Phys. Rev. B **46**, 9270 (1992).
28. T. Hsu, Phys. Rev. B **52**, 9178 (1995).
29. N. B. Kopnin, Sov. Phys. JETP Lett. **27**, 391 (1978).
30. N. B. Kopnin and A. V. Lopatin, Phys. Rev. B **51**, 15291 (1995).
31. M. Eschrig, J. A. Sauls, and D. Rainer, Phys. Rev. B **60**, 10447 (1999).
32. D. I. Khomskii and A. Freimuth, Phys. Rev. Lett. **75**, 1384 (1995).
33. M. V. Feigel'man, V. B. Geshkenbein, A. I. Larkin, and V. M. Vinokur, Sov. Phys. JETP Lett. **62**, 834 (1995).
34. G. Blatter *et al.*, Phys. Rev. Lett. **77**, 566 (1996).